Revised Version

DESY 09-008
MZ-TH/09-03
LPSC 09-17

DESY 09–008, MZ–TH/09–03, LPSC 09–17 ISSN 0418-9833

Open charm hadroproduction and the charm content of the proton

Bernd A. Kniehl* and Gustav Kramer†

II. Institut für Theoretische Physik, Universität Hamburg,

Luruper Chaussee 149, 22761 Hamburg, Germany

Ingo Schienbein‡

Laboratoire de Physique Subatomique et de Cosmologie,

Université Joseph Fourier Grenoble 1, CNRS/IN2P3,

Institut National Polytechnique de Grenoble,

53 avenue des Martyrs, 38026 Grenoble, France

Hubert Spiesberger§

Institut für Physik, Johannes-Gutenberg-Universität,

Staudinger Weg 7, 55099 Mainz, Germany

(Dated: April 27, 2009)

Abstract

We advocate charmed-hadron inclusive hadroproduction as a laboratory to probe intrinsic charm (IC) inside the colliding hadrons. Working at next-to-leading order in the general-mass variable-flavor-number scheme endowed with non-perturbative fragmentation functions recently extracted from a global fit to e^+e^- annihilation data from KEKB, CESR, and LEP1, we first assess the sensitivity of Tevatron data of D^0, D^+, and D^{*+} inclusive production to the IC parameterizations provided by Pumplin *et al.* We then argue that similar data from pp collisions at RHIC would have the potential to discriminate between different IC models provided they reach out to sufficiently large values of transverse momentum.

PACS numbers: 12.38.Bx, 13.85.Ni, 13.87.Fh, 14.40.Nd

*Electronic address: kniehl@desy.de

†Electronic address: gustav.kramer@desy.de

‡Electronic address: schien@lpsc.in2p3.fr

§Electronic address: hspiesb@thep.physik.uni-mainz.de

I. INTRODUCTION

Recently, the inclusive production of charmed hadrons (X_c) at hadron colliders has been the subject of extensive experimental and theoretical studies. The CDF Collaboration measured the differential cross section $\mathrm{d}\sigma/\mathrm{d}p_T$ for the inclusive production of D^0, D^+, D^{*+}, and D_s^+ mesons (and their antiparticles) in $p\overline{p}$ collisions at the Fermilab Tevatron (run II), with center-of-mass energy $\sqrt{s} = 1.96$ TeV, as a function of the transverse momentum (p_T) in the central rapidity (y) region [1]. The PHENIX Collaboration measured non-photonic electron production through charm and bottom decays in pp, dAu, and AuAu collisions at the BNL Relativistic Heavy Ion Collider (RHIC) with $\sqrt{s} = 200$ GeV as a function of p_T [2]. The STAR Collaboration at RHIC presented mid-rapidity open charm spectra from direct reconstruction of $D^0/\overline{D}^0 \to K^{\mp}\pi^{\pm}$ decays in dAu collisions and indirect electron-positron measurements via charm semileptonic decays in pp and dAu collisions at $\sqrt{s} = 200$ GeV [4]. Recently, they also reported results on non-photonic electron production in pp, dAu, and AuAu collisions at $\sqrt{s} = 200$ GeV [3]. Unfortunately, these RHIC data only cover a very limited small-p_T range, where theoretical predictions based on perturbative QCD are difficult.

On the theoretical side, the cross sections for the inclusive production of X_c mesons can be obtained as convolutions of universal parton distribution functions (PDFs) and universal fragmentation functions (FFs) with perturbatively calculable hard-scattering cross sections. The non-perturbative input in form of PDFs and FFs must be known from fits to other processes. The universality of the PDFs and FFs guarantees unique predictions for the cross section of the inclusive production of heavy-flavored hadrons. The results of such calculations for X_c production at the Tevatron have been presented recently by us in Ref. [5] and compared to the CDF data [1]. For all four meson species, D^0, D^+, D^{*+}, and D_s^+, we found good agreement with the data in the sense that the experimental and theoretical errors overlap. For the D^0, D^{*+}, and D_s^+ mesons, many of the central data points fall into the theoretical error band due to scale variation. Only the central data points for the D^+ mesons lie somewhat above it. For the D^0, D^+, and D^{*+} mesons, the central data points tend to overshoot the central theoretical prediction by a factor of about 1.5 at the lower end of the considered p_T range. With the exception of the D_s^+ case, the experimental results are gathered on the upper site of the theoretical error band, corresponding to a small value of

the renormalization scale μ_R and large values of the factorization scales μ_F and μ'_F, related to the initial and final states, respectively.

In our analysis [5], we employed the general-mass variable-flavor-number scheme (GM-VFNS), which combines the zero-mass variable-flavor-number scheme (ZM-VFNS) and the fixed-flavor-number scheme (FFNS). The GM-VFNS is close to the ZM-VFNS, but retains m^2/p_T^2 power terms in the hard-scattering cross sections. Here, m stands for the mass of the charm quark. The calculational details for hadron-hadron collisions were elaborated in our previous works [6]. The characteristic feature of the GM-VFNS is that the charm quark is also treated as an incoming parton originating from the (anti)proton, leading to additional contributions besides those from the light u, d, and s quarks and the gluon. This is quite analogous to the ZM-VFNS, but with the important difference that the power terms are retained in the hard-scattering cross sections. This allows us to apply the GM-VFNS also in the region of intermediate p_T values, $p_T \gtrsim m$. In fact, in Ref. [5], we had $p_T \gtrsim m$.

In Ref. [5], we included $n_f = 4$ active quark flavors and took the charm-quark mass to be $m = 1.5$ GeV. The strong-coupling constant $\alpha_s^{(n_f)}(\mu_R)$ was evaluated in next-to-leading order (NLO) with $\Lambda^{(4)} = 328$ MeV, corresponding to $\alpha_s^{(5)}(m_Z) = 0.1181$. We employed proton PDF set CTEQ6.1M from the Coordinated Theoretical-Experimental Project on QCD (CTEQ) Collaboration [7] and the FFs from Ref. [8]. The default choice for the renormalization and the initial- and final-state factorization scales was $\mu_R = \mu_F = \mu'_F = m_T$, where $m_T = \sqrt{p_T^2 + m^2}$ is the transverse mass.

Compared to our previous work [5], we have now much more reliable FFs for the transitions $u, d, s, c, g \to X_c$ at our disposal. The FFs used in Ref. [5] were determined by fitting the fractional-energy spectra of the hadrons X_c measured by the OPAL Collaboration [9, 10] in e^+e^- annihilation on the Z-boson resonance at the CERN LEP1 collider. These data had rather large experimental errors and the disadvantage of being at a rather large scale $\mu'_F = M_Z$, far away from the scales of X_c production in $p\overline{p}$ collisions at the Tevatron, which typically correspond to p_T values below 25 GeV. In the meantime, new data on charmed-meson production with much higher accuracy were presented by the CLEO Collaboraton [11] at CESR and by the Belle Collaboration [12] at the KEK collider for B physics (KEKB). These data offered us the opportunity to determine the non-perturbative initial condition of the FFs much more accurately. The data from CLEO [11] and Belle [12] are located much closer to the threshold $\sqrt{s} = 2m$ of the transition $c \to X_c$ than those from

OPAL [9, 10]. The scale of the CLEO [11] and Belle [12] data is set by the c.m. energy $\sqrt{s} = 10.5$ GeV. Recently, Kneesch and three of us extracted from these data FFs for D^0, D^+, and D^{*+} mesons; the details may be found in Ref. [13].

Another important ingredient for the theoretical description of inclusive X_c production are the parton distribution functions (PDFs). Let $f_a(x, \mu_F)$ denote the PDF of parton a inside the proton at momentum fraction x and factorization scale μ_F. At short distances, corresponding to large values of μ_F, the scale dependence is determined by the QCD evolution equations with perturbatively calculable evolution kernels. So, the PDFs are fully determined by their functional forms in x specified at a fixed scale $\mu_F = \mu_0$ provided μ_0 is large enough to be in the region where perturbative QCD is supposed to the valid. In most applications, μ_0 is chosen to be of order 1–2 GeV, which is at the borderline between the short-distance (perturbative) and long-distance (non-perturbative) regions. The PDFs of the gluon and the light quarks ($a = g, u, d, s$) are non-perturbative. They are obtained phenomenologically through global QCD analyses, in which the theoretical predictions are compared with a wide range of experimental data on hard processes [7, 14, 15].

The cross sections of inclusive charmed-meson production in the GM-VFNS depend heavily on the PDF of the charm quark and less on those of the light quarks. In the following, we use the short-hand notation $c(x, \mu_F) = f_c(x, \mu_F)$. In the global analyses of Refs. [7, 14, 15] and many others [16], the charm quark is considered a parton. It is characterized by the PDF $c(x, \mu_F)$ that is defined for $\mu_F > m$. In common global QCD analyses at NLO in the $\overline{\text{MS}}$ scheme, the charm quark is considered as a heavy quark, and the ansatz $c(x, \mu_0) = 0$ with $\mu_0 = m$ is assumed as the initial condition for calculating $c(x, \mu_F)$ at higher factorization scales $\mu_F > \mu_0$. This is usually referred to as the radiatively-generated-charm approach. In the global analyses cited above, this ansatz implies that the charm parton does not have any independent degrees of freedom in the parton parameter space, *i.e.*, $c(x, \mu_F)$ is perturbatively determined by the gluon and light-quark parton parameters.

However, a purely perturbative treatment of the heavy quarks might not be adequate. This is even more true for the charm quark with mass $m \approx 1.5$ GeV, which is not much larger than typical hadronic scales of a few hundred MeV. In fact, there exists the possibility, that $c(x, \mu_0) \neq 0$. Actually, for many years, non-perturbative models exist that give non-zero predictions for $c(x, \mu_0)$ at some initial factorization scales $\mu_0 = \mathcal{O}(m)$ [17, 18]. The model of Ref. [17] was also analyzed in the framework of the FFNS [19]. In this connection, the

notion intrinsic charm (IC) has become customary. The IC models of Refs. [17, 18] and a third one, which will be specified in a later section, were put to a stringent test by extending the recent CTEQ6.5 global analysis [14] so that the charm sector has its own independent degrees of freedom at the initial factorization scale $\mu_0 = m$ [20]. As a natural extension of the CTEQ6.5 analysis [14], Pumplin *et al.* [20] determined the range of magnitude of IC that is consistent with an up-to-date global analysis of hard-scattering data with various assumptions on the shape of the x distribution of IC at a low factorization scale.

The authors of Ref. [20] found the IC of the light-cone models [17, 18] to be compatible with the global data sample for magnitudes ranging from zero up to three times of what had been estimated in more model-dependent investigations. In these models, there can be a large enhancement of $c(x, \mu_F)$ at $x > 0.1$, relative to previous analyses that have no IC. The enhancement persists to rather large scales μ_F, up to 100 GeV. Therefore, these nonzero IC contributions can have an important effect on charm-initiated processes at HERA, RHIC, the Tevatron, and the LHC. Of course, at hadron colliders, the charm production cross section would be sensitive to $c(x, \mu_F)$ at $x > 0.1$ only at sufficiently large values of $x_T = 2p_T/\sqrt{s}$. For example, the cross section data at the Tevatron [1] only cover the range $p_T < 25$ GeV, so that $x_T < 0.025$, which is too small to be sensitive to IC contributions at $x > 0.1$. Only at RHIC, where $\sqrt{s}$ is a factor of 10 smaller, we may expect sufficient sensitivity. At given values of $\sqrt{s}$ and p_T, the sensitivity to $c(x, \mu_F)$ at large values of x could be further enhanced by performing measurements at large values of $|y|$, *i.e.* in the extreme forward or backward regions [21].

The obvious data that could provide us with information on the IC contribution, would be those on the charm structure function F_2^c measured at HERA. But these data are already used in the global analysis [20]. Unfortunately, they do not have a significant effect because of the rather large experimental errors and because the data are mostly located at small values of x. A comparison of such data with results from earlier CTEQ global analyses may be found in Ref. [22].

After these general remarks, it is clear that it is interesting to study cross sections of inclusive charmed-meson production at RHIC ($\sqrt{s} = 200$ GeV) and the Tevatron ($\sqrt{s} = 1.96$ TeV) more closely and to establish those kinematic regions which are sensitive to the IC component of the proton. For this purpose, we adopt the GM-VFNS approach outlined in Ref. [5, 6]. We first compare the D^0, D^+, and D^{*+} production data from Ref. [1] to

NLO predictions evaluated with the respective FF sets [13] so as to test the latter (with or without IC). Then, we present results for the D^0 production cross section under Tevatron and RHIC experimental conditions assuming the six IC scenarios introduced in Ref. [20].

The outline of this paper is as follows. In Sec. II, we briefly review the FFs determined in Ref. [13]. In Sec. III, we describe the three IC models investigated in Ref. [20] as much as is needed to understand our final results. In Sec. IV, we present our NLO predictions for inclusive X_c production in $p\overline{p}$ and pp collisions. Section V contains a summary and an outlook.

II. FRAGMENTATION FUNCTIONS FOR CHARMED MESONS

For our calculation of the differential cross section $\mathrm{d}^2\sigma/(\mathrm{d}p_T\,\mathrm{d}y)$ of $p + p(\overline{p}) \to X_c + X$, where $X_c = D^0, D^+, D^{*+}$ and X stands for the residual final state, a crucial ingredient is the non-perturbative FFs for the transitions $a \to X_c$, where $a = g, u, \overline{u}, d, \overline{d}, s, \overline{s}, c, \overline{c}$. For $X_c = D^{*+}$, such FFs were extracted at LO and NLO in the modified minimal-subtraction ($\overline{\mathrm{MS}}$) factorization scheme with $n_f = 5$ massless quark flavors several years ago [23] from the distributions $\mathrm{d}\sigma/\mathrm{d}x$ in scaled energy $x = 2E/\sqrt{s}$ of the cross sections of $e^+ + e^- \to D^{*+} + X$ measured by the ALEPH [24] and OPAL [10] Collaborations at LEP1. Two of us [25] extended the analysis of Ref. [23] to include $X_c = D^0, D^+, D_s^+, \Lambda_c^+$ by fitting appropriate OPAL data [9]. Besides the total X_c yield, which receives contributions from $Z \to c\overline{c}$ and $Z \to b\overline{b}$ decays as well as from light-quark and gluon fragmentation, the ALEPH and OPAL Collaborations separately specified the contributions due to tagged $Z \to b\overline{b}$ events yielding X_b hadrons, which then weakly decay to X_c hadrons. The contribution due to the fragmentation of primary charm quarks into X_c hadrons approximately corresponds to the difference of these two measured distributions.

In Refs. [23, 25], the starting point μ_0 for the DGLAP evolution of the $a \to X_c$ FFs in the factorization scale μ_F' were taken to be $\mu = 2m$ with $m = 1.5$ GeV for $a = g, u, \overline{u}, d, \overline{d}, s, \overline{s}$ and $\mu = 2m_b$ with $m_b = 5$ GeV for $a = b, \overline{b}$. The FFs for $a = g, u, \overline{u}, d, \overline{d}, s, \overline{s}$ were assumed to vanish at $\mu_F' = \mu_0$ and generated through DGLAP evolution to larger values of μ_F'. For consistency with the $\overline{\mathrm{MS}}$ prescription for the PDFs, these fits of the FFs were repeated for the choice $\mu_0 = m, m_b$ in Ref. [8]. These determinations of X_c FFs [8, 23, 25] were all based solely on data from the Z-boson resonance. In these data, the effects of finite quark and

hadron masses were greatly suppressed and could safely be neglected.

The most recent fits for $X_c = D^0, D^+, D^{*+}$ reported in Ref. [13] include, beside the OPAL [9, 10] and ALEPH [24] data, much more precise data from CLEO [11] and Belle [12]. They offered us the opportunity to further constrain the charmed-hadron FFs and test their scaling violations. However, the lower c.m. energies of the CLEO [11] and Belle [12] data necessitates the incorporation of quark and hadron mass effects, which are then no longer negligible, into the formalism. The GM-VFNS, which is also the basis of the computation of the cross section of $p + \overline{p} \to X_c + X$ in Refs. [5, 6], provides the appropriate theoretical framework also for this (see Ref. [13] for details). We adopted the values of μ_0 and m from Ref. [8].

In this framework, new FFs for D^0, D^+, and D^{*+} mesons were determined through global fits to all available e^+e^- annihilation data, from Belle [12], CLEO [11], ALEPH [24], and OPAL [9, 10]. In contrast to the situation at the Z-boson resonance, we had to take into account the effect of electromagnetic initial-state radiation on the Belle and CLEO data, which distorts the distribution in scaled momentum $x_p = 2p/\sqrt{s}$ of the cross section for continuum production in a non-negligible way [13]. We found that the global fits suffer from the fact that the Belle and CLEO data tend to drive the average of x of the $c \to X_c$ FFs to larger values, which leads to a somewhat worse description of the ALEPH and OPAL data. Since the $b \to X_c$ FFs are only indirectly constrained by the Belle and CLEO data, namely via their contribution to the DGLAP evolution, their forms are only feebly affected by the inclusion of these data in the fits. In other words, the $b \to X_c$ FFs are essentially fixed by the ALEPH and OPAL data alone. It was found that hadron mass effects are more important than quark mass effects in the global fits. In fact, they are indispensable for fitting the lower tails of the x_p distributions from Belle and CLEO

The z distributions of the c and b quark FFs at their starting scales were assumed to obey the Bowler ansatz [26]

$$D_a^{X_c}(z, \mu_0) = N z^{-(1+\gamma^2)} (1-z)^a \mathrm{e}^{-\gamma^2/z}, \tag{1}$$

with three parameters N, a, and γ. Specifically, the fitting procedure was as follows. At the scale $\mu_0 = m = 1.5$ GeV, the c-quark FF was taken to be of the form of Eq. (1), while the FFs of the light quarks q ($q = u, d, s$) and the gluon were set to zero. Then these FFs were evolved to higher scales μ_F' using the DGLAP equations with $n_f = 4$ active quark flavors

and $\Lambda^{(4)}_{\overline{\rm MS}} = 321$ MeV. When the scale μ'_F reached the threshold value $\mu'_F = m_b = 5.0$ GeV, the bottom flavor was activated and its FF was introduced in the Bowler form of Eq. (1). The evolution to higher scales μ'_F was then performed with $n_f = 5$ and $\Lambda^{(5)}_{\overline{\rm MS}} = 221$ MeV. The values of the Bowler parameters N_c, a_c, and γ_c for $c \to X_c$ and N_b, a_b, and γ_b for $b \to X_c$ thus obtained may be found in Tables 1, 2, and 3 of Ref. [13] for the D^0, D^+, and D^{*+} mesons, respectively, together with the achieved values of χ^2 per d.o.f. ($\overline{\chi^2}$). The $\overline{\chi^2}$ values differ somewhat for the three D-meson species, but they are all acceptable. The smallest $\overline{\chi^2}$ value was obtained for the D^+ meson.

III. PDFS WITH INTRINSIC CHARM

In a recent paper [20], Pumplin *et al.* extended the up-to-date CTEQ6.5 global analysis [14] to include a charm sector with nonzero $c(x, \mu_0)$ at the initial factorization scale $\mu_0 = m$. For this purpose, they considered three scenarios. The first two scenarios are based on the light-cone Fock-space picture of nucleon structure formulated in more detail by Brodsky [27]. In this picture, IC is mainly present at large momentum fraction x, because states containing heavy quarks are suppressed according to their off-shell distance, which is proportional to $(p_T^2 + m^2)/x$. Thus, components with large m appear preferentially at large x. A wide variety of light-cone models predict similar shapes in x, as has been shown recently [28]. Specifically, the light-cone models considered in Ref. [20] include the original model of Brodsky, Hoyer, Peterson, and Sakai (BHPS) [17] and the so-called meson-cloud picture [18], in which the IC arises from virtual low-mass meson-plus-baryon components of the proton, such as $\overline{D}^0 \Lambda_c^+$. The meson-cloud model also predicts a difference between $c(x, \mu'_F)$ and $\overline{c}(x, \mu'_F)$ and so provides an estimate of the possible charm/anticharm difference.

Unfortunately, the light-cone formalism does not allow us to calculate the normalization of the $uudc\overline{c}$ components [28], although estimates of the order of 1% were reported in the literature [18, 29]. Therefore, in Ref. [20], the magnitude of IC is determined by comparison with data incorporated in the global fit.

The x dependence originating in the BHPS model [17] is

$$c(x, \mu_0) = \overline{c}(x, \mu_0) = A x^2 [6x(1+x)\ln x + (1-x)(1+10x+x^2)]. \qquad (2)$$

In Eq. (2), $\mu_0 = m$ with $m = 1.3$ GeV and the normalization constant A is treated as a free

parameter in the fit. Its magnitude is controlled by the average $c + \overline{c}$ momentum fraction,

$$\langle x \rangle_{c+\overline{c}} = \int_0^1 \mathrm{d}x \, x[c(x,\mu_0) + \overline{c}(x,\mu_0)]. \tag{3}$$

The exact x dependence predicted by the meson-cloud model cannot be given by a simple formula. However, it was shown in Ref. [28] that the charm distributions in this model can be very well approximated by

$$\begin{aligned} c(x,\mu_0) &= A x^{1.897}(1-x)^{6.095}, \\ \overline{c}(x,\mu_0) &= \overline{A} x^{2.511}(1-x)^{4.929}, \end{aligned} \tag{4}$$

where the normalization constants A and $\overline{A}$ are constrained by the quark number sum rule,

$$\int_0^1 \mathrm{d}x \, [c(x,\mu_0) - \overline{c}(x,\mu_0)] = 0, \tag{5}$$

which fixes $A/\overline{A}$. The overall magnitude of IC is again determined in the global analysis.

As a third scenario, Pumplin *et al.* [20] studied a purely phenomenological scenario in which the shape of the charm distribution is sea-like, *i.e.* similar to those of the light-flavor sea quarks, except for an overall mass suppression. In particular, they assumed that $c(x,\mu_0) = \overline{c}(x,\mu_0) \propto \overline{u}(x,\mu_0) + \overline{d}(x,\mu_0)$ at $\mu_0 = m$.

The $c(x,\mu_0)$ and $\overline{c}(x,\mu_0)$ functions of the BHPS, meson-cloud, and sea-like models discussed above are used in Ref. [20] as input for the general-mass perturbative QCD evolution as explained in Ref. [14]. Then, the range of the IC magnitude is determined to be consistent with the global data fit. The quality of each global fit is measured by χ^2_{global}, which is shown in Fig. 1 of Ref. [20] as a function of $\langle x \rangle_{c+\overline{c}}$ for the three models. From this figure, one can see that in the lower range, $0 < \langle x \rangle_{c+\overline{c}} \lesssim 0.01$, χ^2_{global} varies very little, *i.e.* the fit is very insensitive to $\langle x \rangle_{c+\overline{c}}$ in this interval. This means that the global analysis of the hard-scattering data gives no evidence either for or against IC up to $\langle x \rangle_{c+\overline{c}} \approx 0.01$. For $\langle x \rangle_{c+\overline{c}} > 0.01$, the curves for the three models in Fig. 1 of Ref. [20] rise steeply with $\langle x \rangle_{c+\overline{c}}$. $\chi^2_{\mathrm{global}} \approx 3450$ represents a marginal fit in each model, beyond which the quality of the fit becomes unacceptable according to the procedure established in Refs. [7, 14]. This criterion is based on the fact that one or more of the individual experiments in the global fit is no longer fitted within the 90% confidence level. For comparison, the fit with no IC yields $\chi^2_{\mathrm{global}} \approx 3330$. The $\langle x \rangle_{c+\overline{c}}$ distributions of χ^2_{global} achieved in the BHPS, meson-cloud, and sea-like models reach the marginal-fit limit of 3450 at 2.0%, 1.8%, and 2.4%, respectively.

The authors of Ref. [20] studied also the typical, more moderate $\langle x\rangle_{c+\overline{c}}$ values 0.57%, 0.96%, and 1.1% in the same order. The x dependences of $c(x,\mu_F)$ and $\overline{c}(x,\mu_F)$ obtained in the three models are shown for the two values of $\langle x\rangle_{c+\overline{c}}$ mentioned above and for various values of μ_F in Figs. 2–4 of Ref. [20] and are compared there with the zero-IC result of the CTEQ6.5 fit. From these figures one notices that, in the two light-cone models, IC leads to an enhancement of $c(x,\mu_F)$ and $\overline{c}(x,\mu_F)$ at $x > 0.1$ relative to the PDF analysis with zero IC, while the deviation is small for $x < 0.1$. In the sea-like model, there is also a significant enhancement of $c(x,\mu_F)$ and $\overline{c}(x,\mu_F)$ relative to the zero-IC PDF. In this case, the enhancement is spread more broadly in x, roughly over the region $0.01 < x < 0.50$.

The six PDF sets constructed with IC, corresponding to the three models with two values of $\langle x\rangle_{c+\overline{c}}$ each, which are designated by CTEQ6.5C in Ref. [20], are available together with the corresponding zero-IC PDF set via the LHAPDF standard [16] as seven members, which we denote as CTEQ6.5Cn with $n = 0, 1, 2, 3, 4, 5, 6$. Specifically, $n = 0$ stands for zero IC, $n = 1, 2$ for the BHPS model with $\langle x\rangle_{c+\overline{c}} = 0.57\%, 2.0\%$, $n = 3, 4$ for the meson-cloud model with $\langle x\rangle_{c+\overline{c}} = 0.96\%, 1.8\%$, and $n = 5, 6$ for the sea-like model with $\langle x\rangle_{c+\overline{c}} = 1.1\%, 2.4\%$.

IV. COMPARISON WITH CDF DATA AND PREDICTIONS FOR RHIC

A. Predictions for CDF

In this section, we present our predictions for the differential cross section $\mathrm{d}^2\sigma/(\mathrm{d}p_T\,\mathrm{d}y)$ of $p + \overline{p} \to X_c + X$ with $X_c = D^0, D^+, D^{*+}$ at NLO in the GM-VFNS. The calculation proceeds as outlined in Ref. [6] with the modifications explained in Sec. II.

The NLO cross section consists of three classes of contributions.

1. Class (i) contains all the partonic subprocesses with a $c, \overline{c} \to X_c$ transition in the final state that have only light partons $(g, q, \overline{q})$ in the initial state, the possible pairings being gg, gq, $g\bar{q}$, and $q\bar{q}$.

2. Class (ii) contains all the partonic subprocesses with a $c, \overline{c} \to X_c$ transition in the final state that also have c or $\overline{c}$ quarks in the initial state, the possible pairings being gc, $g\overline{c}$, qc, $q\overline{c}$, $\overline{q}c$, $\overline{qc}$, and $c\overline{c}$.

3. Class (iii) contains all the partonic subprocesses with a $g, q, \bar{q} \to X_c$ transition in the

final state.

The contributions of classes (ii) and (iii) are calculated in the ZM-VFNS using the hard-scattering cross sections usually used for the inclusive production of light mesons [30]. The light-quark fragmentation contributions are negligible. However, gluon fragmentation contributes significantly, as was first noticed in our previous work [5].

As was shown in Ref. [6], the m dependence of the class-(i) contribution is greatly screened in the full cross section because the latter is dominated by the contributions of classes (ii) and (iii), which are calculated with $m = 0$. In fact, the bulk of the contribution is due to class (ii), which provides a handle on the $c(x, \mu_F)$ and $\overline{c}(x, \mu_F)$ and thus on IC.

The CDF data [1] come as distributions $\mathrm{d}\sigma/\mathrm{d}p_T$ at $\sqrt{s} = 1.96$ TeV with y integrated over the range $|y| \leq 1$. For each X_c meson, the particle and antiparticle contributions are averaged. We work in the GM-VFNS with $n_f = 4$ thus excluding X_c hadrons from X_b-hadron decays, which are vetoed in the CDF analysis [1]. For the comparison with the CDF data, we use set CTEQ6.5 of proton PDFs [14] without IC (see Sec. III), and set global-GM of X_c FFs [13] (see Sec. II). We adopt the value $\Lambda^{(4)}_{\overline{\mathrm{MS}}} = 328$ MeV, which yields $\alpha_s^{(5)}(M_Z) = 0.1181$, from Ref. [14] and the values $m = 1.5$ GeV and $m_b = 5$ GeV from Ref. [13]. There is a slight mismatch of the input parameters n_f, $\Lambda^{(4)}_{\overline{\mathrm{MS}}}$, m, and m_b, since Ref. [14] uses $n_f = 5$, $m = 1.3$ GeV and $m_b = 4.5$ GeV and Ref. [13] uses $n_f = 5$ and $\Lambda^{(4)}_{\overline{\mathrm{MS}}} = 321$ MeV. The difference between the values of $\Lambda^{(4)}_{\overline{\mathrm{MS}}}$ is certainly insignificant. The different choices for m and m_b, which set the flavor thresholds, will feebly affect the evolution of the strong-coupling constant, the PDFs, and the FFs. In order to conservatively estimate the scale uncertainty, we set $\mu_R = \xi_R m_T$, $\mu_F = \mu'_F = \xi_F m_T$, independently vary ξ_R and ξ_F in the range $1/2 < \xi_R, \xi_F < 2$, and determine the maximum upward and downward deviations from our default predictions, for $\xi_R = \xi_F = 1$.

The theoretical predictions evaluated with the CTEQ6.5 PDFs [14] and the new FFs [13] are compared with the CDF data [1] on an absolute scale in Fig. 1 and in the data-over-theory representation with respect to the default results in Fig. 2. The three frames in each figure refer to the D^0, D^+, and D^{*+} mesons; in each frame, the theoretical uncertainty due to the scale variation described above is indicated by the dashed lines. In all cases, we find that the agreement with the data is improved relative to our previous analysis [5], as may be seen by comparing Figs. 1 and 2 with Figs. 1 and 2 in Ref. [5]. In fact, the D^0 data, except for the smallest-p_T point, and the D^+ data agree with our default predictions

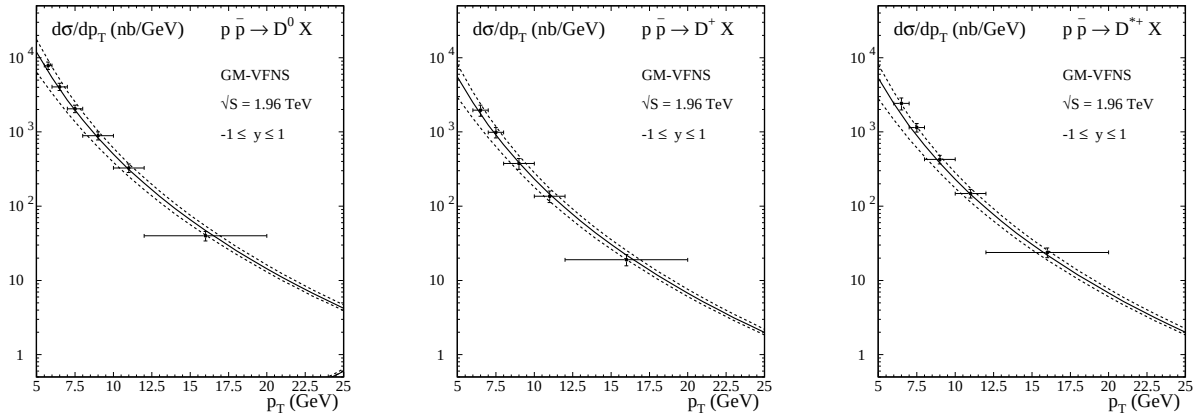

(a) (b) (c)

FIG. 1: p_T distributions $\mathrm{d}\sigma/\mathrm{d}p_T$ of $p + \overline{p} \to X_c + X$ with (a) $X_c = D^0$, (b) $X_c = D^+$, and (c) $X_c = D^{*+}$ for $\sqrt{s} = 1.96$ TeV and $|y| < 1$ evaluated at NLO in the GM-VFNS using the FFs of Ref. [13] in comparison with experimental data from CDF [1]. The solid lines represents the default predictions, for $\xi_R = \xi_F = 1$, and the dashed lines indicate the maximum deviations for independent variations in the range $1/2 < \xi_R, \xi_F < 2$.

within the experimental errors. This is also true for the D^{*+} data, except for the two small-p_T points. This improvement may be attributed to the advancement in our knowledge of charmed-meson FFs [13], which now also includes detailed information from the B factories, while the previously used FF set was solely based on LEP1 data [8].

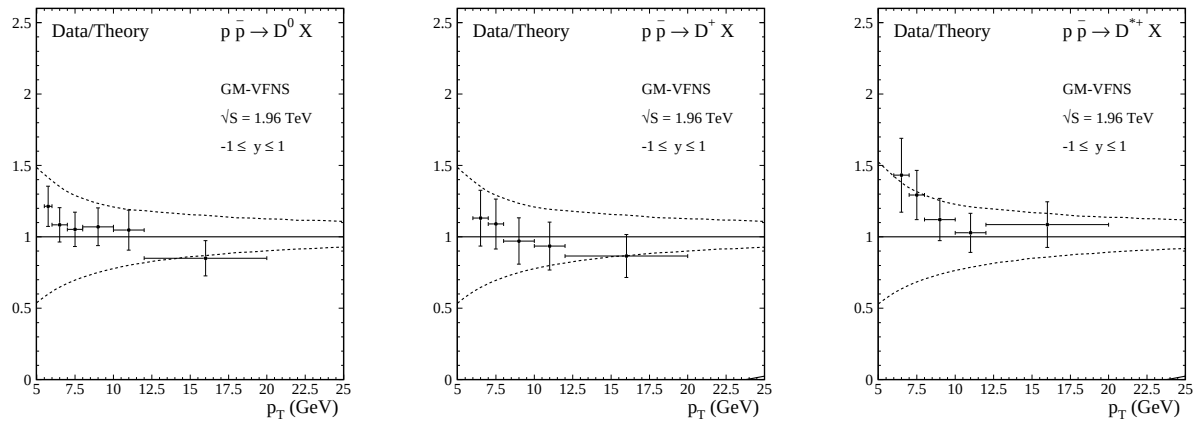

(a) (b) (c)

FIG. 2: Same as in Figs. 1(a)–(c), but normalized to the default predictions.

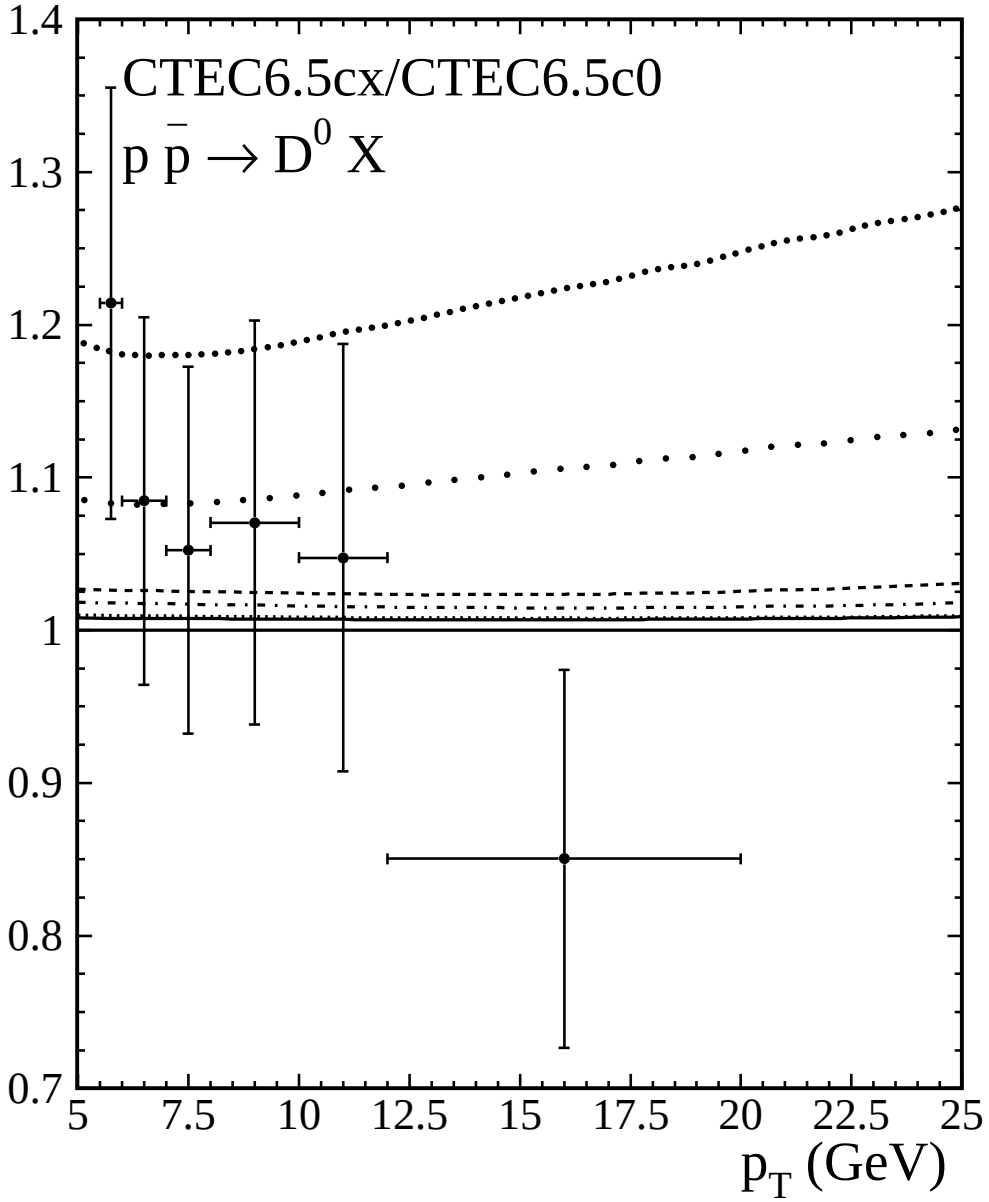

FIG. 3: Same as in Fig. 2(a), but including besides the default prediction those evaluated with the IC parameterizations from Ref. [20] for $n = 1$ (solid line), 2 (dashed line), 3 (densely dotted line), 4 (dot-dashed line), 5 (scarcely dotted line), 6 (dotted line).

In the following, we take the point of view that the FFs for the X_c mesons are sufficiently well known and ask the question whether the CDF data can discriminate between the various CTEQ6.5 PDF sets endowed with IC. For brevity, we only present our results for the case of the D^0 meson, which yields the largest cross section; the results for the D^+ and D^{*+} mesons are very similar. Specifically, we repeat the calculation of the central prediction in Fig. 1(a) in turn with PDF sets CTEQ6.5Cn for $n = 1, \ldots, 6$ and normalize the outcome to the default prediction with zero IC of Fig. 1(a). The results are shown in Fig. 3. We observe that the ratios for $n = 1, 2, 3, 4$ lie very close to unity, the largest deviation being 2%. Only the ratios for $n = 5, 6$ significantly deviate from unity. In fact, for $n = 5$ the ratio is around 1.1, and for $n = 6$ it ranges between 1.17 and 1.27 in the considered p_T range. This finding is easy to understand. The x values dominantly contributing to the production cross section at the Tevatron are typically rather small, *e.g.* $x < x_T \approx 0.025$ for $p_T = 25$ GeV. In this x range, IC is greatly suppressed for $n = 1, 2, 3, 4$, while the IC for $n = 5, 6$ is significant for $x > 10^{-3}$. The IC for $n = 6$, with $\langle x \rangle_{c+\overline{c}} = 0.024$, is more pronounced than that for $n = 5$, with $\langle x \rangle_{c+\overline{c}} = 0.011$, which explains the hierarchy of the respective ratios in Fig. 3. We conclude from Fig. 3 that the size of the IC enhancement is comparable to the errors on the CDF data only for $n = 5, 6$. In fact, the two large-p_T data points from CDF tend to disfavor the sea-like IC implemented for $n = 6$, although a firm statement would be premature. On the other hand, the effects due the IC of the BHPS ($n = 1, 2$) or meson-cloud ($n = 3, 4$) models are too feeble to be resolved by the presently available CDF data. In order to obtain a handle on these types of IC, one needs data at considerably larger values of p_T, where the deviations from the zero-IC prediction are sufficiently large. Of course, the cross sections will be much smaller there and hard to measure with sufficient accuracy.

However, one should keep in mind that the CDF analysis of Ref. [1] is merely based on 5.8 pb^{-1} of data recorded in February and March 2002. Since then the integrated luminosity of run II has increased by more than a factor of 1000, exceeding 6 fb^{-1} as it does. Therefore, we conclude this section by exploring the p_T range beyond 25 GeV, up to 75 GeV, assuming the data to be taken in the central tracking region, $|y| < 1$, as before. The respective extensions of Figs. 1(a) and 3 are presented as Figs. 4(a) and (b). From Fig. 4(a), we read off that the cross section decreases from 5 to 5×10^{-3} nb/GeV as p_T runs from 25 to 75 GeV, and that the theoretical uncertainty ranges from small to negligible. Comparing Fig. 4(b) with Fig. 3, we observe that, in the BHPS and meson-cloud models, the sensitivity

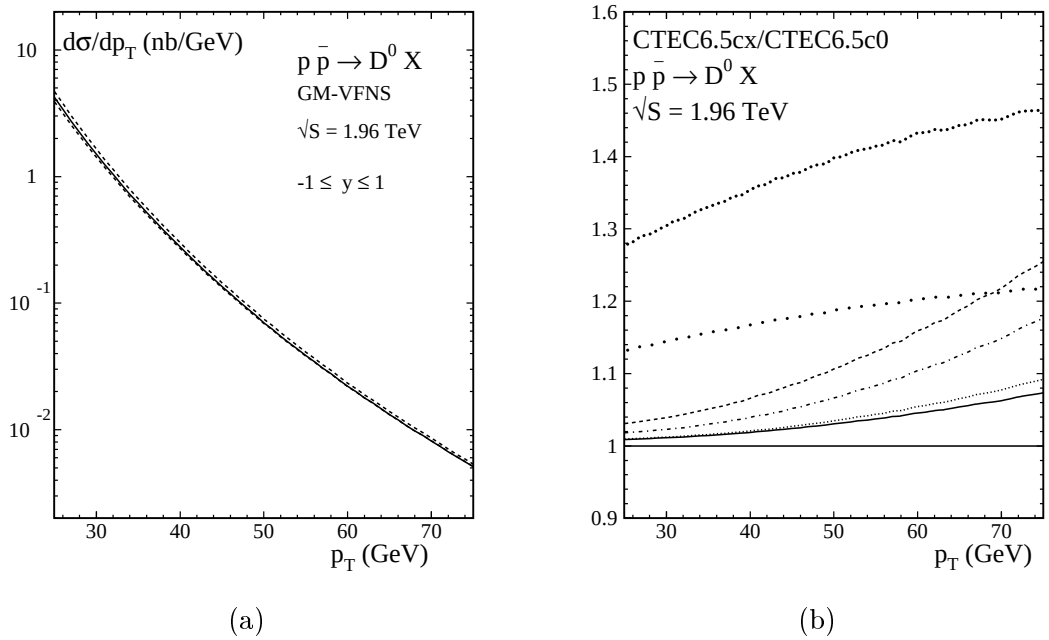

(a) (b)

FIG. 4: Same as in Figs. 1(a) and 3, but for 25 GeV $< p_T <$ 75 GeV.

to IC is dramatically increased as p_T runs from 25 to 75 GeV, while it reaches some level of saturation in the sea-like model. We conclude that the measurements of the cross section distributions $\mathrm{d}\sigma/\mathrm{d}p_T$ of $p\overline{p} \to X_c + X$ based on the full data sample to be collected at the Tevatron by the end of run II would have the potential to yield useful constraints on IC.

B. Predictions for RHIC

Instead of measuring the cross sections at much larger values of p_T with the CDF and D0 detectors at the Tevatron, it may be advantageous to lower the c.m. energy to decrease x_T in the considered p_T range. A collider with smaller c.m. energy is in operation, namely RHIC with $\sqrt{s} = 200$ GeV, where the cross section distributions $\mathrm{d}\sigma/\mathrm{d}p_T$ of $pp \to X_c + X$ could be measured. So far, only the STAR Collaboration has published X_c production data, namely for $d\mathrm{Au} \to D^0 + X$ with $p_T < 2.5$ GeV [4]. We encourage STAR and PHENIX to also study $pp \to D^0 + X$ at larger values of p_T.

The calculations of $\mathrm{d}^2\sigma/(\mathrm{d}p_T\,\mathrm{d}y)$ for $pp \to X_c + X$ at RHIC are completely analogous to the Tevatron case. We only need to replace the antiproton PDFs by proton PDFs and put $\sqrt{s} = 200$ GeV. We again integrate y over the range $|y| < 1$. In Fig. 5, we show $\mathrm{d}\sigma/\mathrm{d}p_T$ as a

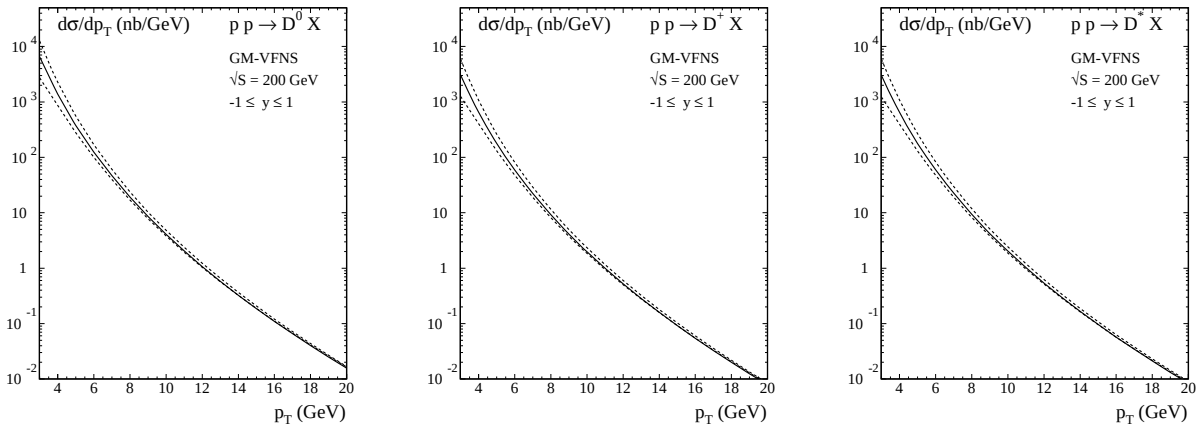

(a) (b) (c)

FIG. 5: Same as in Fig. 1, but for pp collisions with $\sqrt{s} = 200$ GeV.

function of p_T in the range 3 GeV $< p_T <$ 20 GeV for $X_c = D^0, D^+, D^{*+}$. The results for D^+ and D^{*+} are very similar, while that for D^0 has a similar shape, but differs in normalization. In fact, the D^{*+} to D^0 cross section ratio ranges from 0.46 to 0.52 in the considered p_T range. As in the case of the Tevatron, the cross sections of $pp \to X_c + X$ at RHIC rapidly fall with increasing value of p_T, by the factor 2.4×10^{-6} as p_T runs from 3 GeV to 20 GeV. Thus, it might be difficult to measure these cross sections in the upper part of the considered p_T range.

We now repeat the analysis for the D^0 meson in Fig. 5 using the various PDF sets with IC, CTEQ6.5Cn with $n = 1, 2, 3, 4, 5, 6$. The results, normalized to the calculation for $n = 0$, are shown in Fig. 6. Here we observe a pattern familiar from the Tevatron case in Fig. 3, except that now these ratios are much larger. In fact, the results for $n = 2, 4$ steeply rise with increasing value of p_T, reaching values of about 3 and 2.8 at $p_T = 20$ GeV. The results for $n = 1, 3$ exhibit less dramatic rises because the IC is weaker in these cases. Comparing Figs. 3 and 6, we conclude that RHIC offers a much higher sensitivity to IC as implemented in CTEQ6.5Cn with $n = 1, \ldots, 4$ than the Tevatron. On the other hand, the results for $n = 5, 6$ at RHIC are rather similar to those at the Tevatron, being almost independent of p_T. But also here, the relative deviation from the zero-IC case is stronger for RHIC.

Unfortunately, in contrast to the Tevatron, RHIC measurements at $\sqrt{s} = 200$ GeV will be limited by low luminosity. This key limitation makes the observation of high-p_T X_c production at this RHIC energy rather unrealistic. The high-energy pp mode of RHIC, with

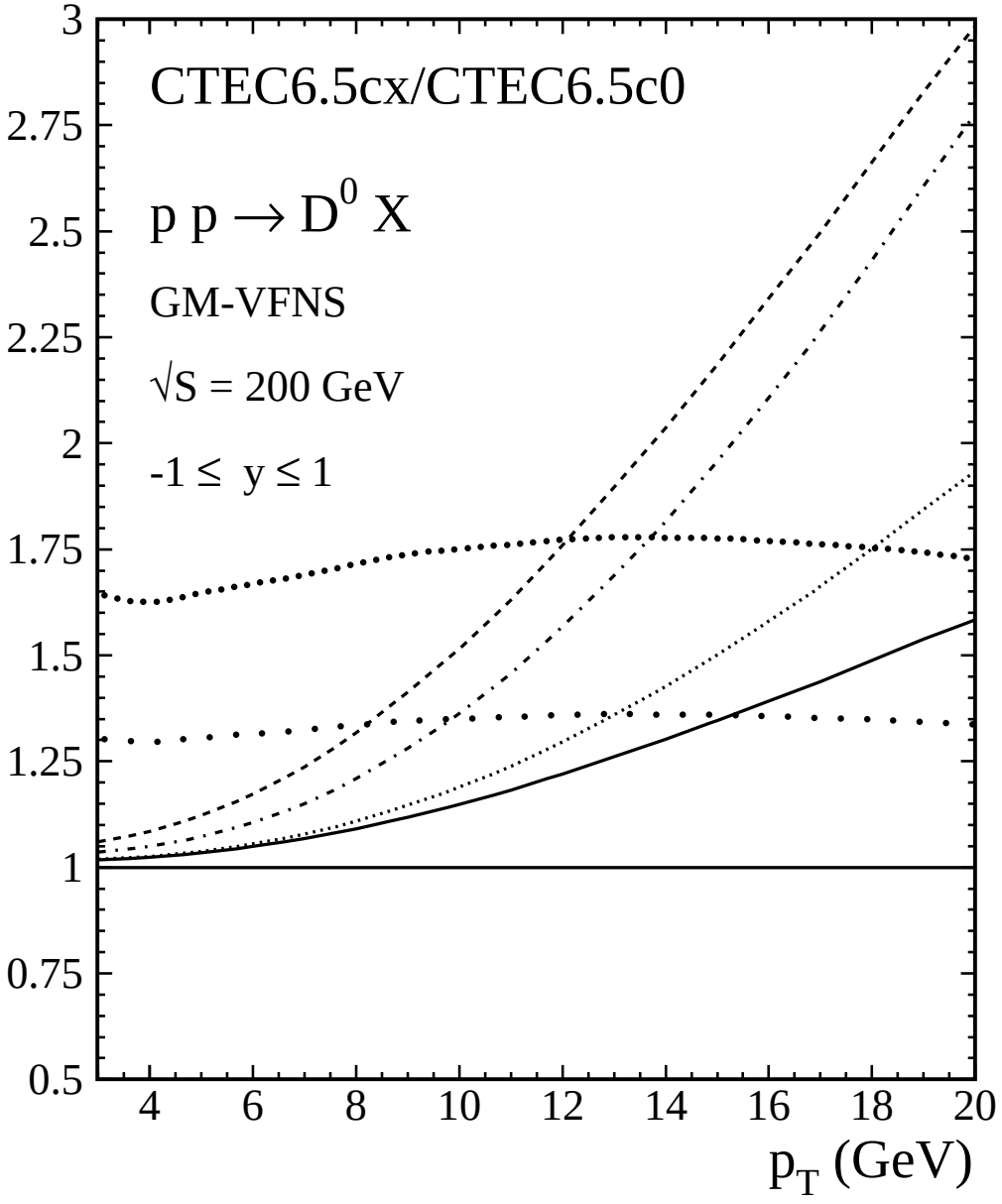

FIG. 6: Same as in Fig. 3, but for pp collisions with $\sqrt{s} = 200$ GeV.

$\sqrt{s} = 500$ GeV, will accrue more luminosity, perhaps 200–400 pb^{-1}. However, this will happen at the expense of lowering the accessible x values and, thus, of reducing the relative IC effects on the cross sections, especially for the BHPS and meson-cloud models. In order to assess the trade-off between higher luminosity and smaller relative shifts in the cross sections, we repeat the D^0-meson analysis for the 500 GeV mode of RHIC. The results are

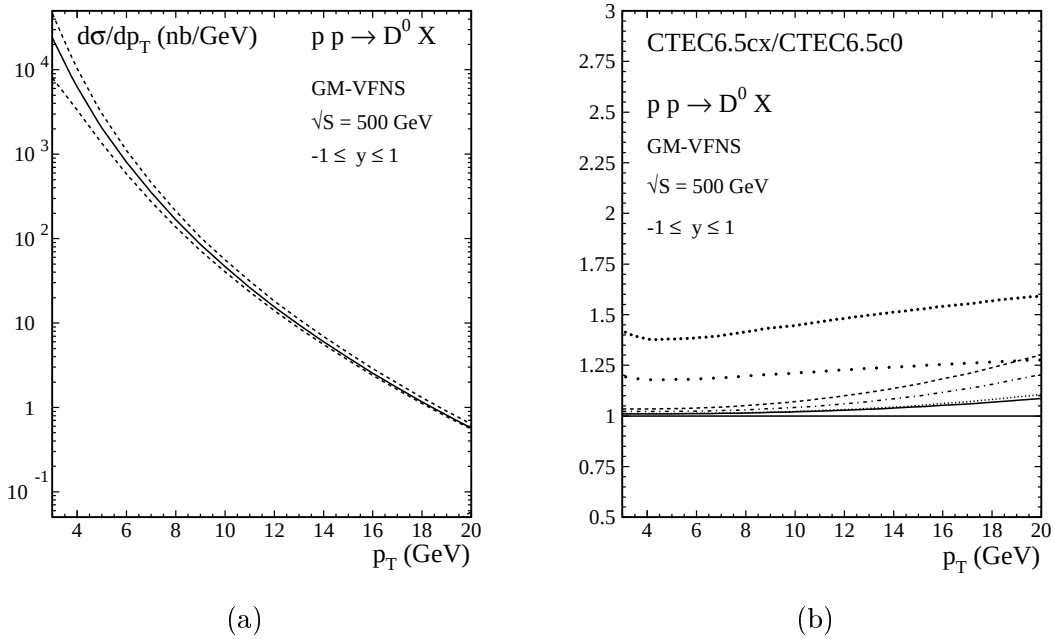

(a) (b)

FIG. 7: Same as in Figs. 5(a) and 6, but for $\sqrt{s} = 500$ GeV.

shown in Figs. 7(a) and (b), which should be compared with Figs. 5(a) and 6, respectively. We observe that, as one passes from 200 GeV to 500 GeV, the cross section is increased by a factor of 3.6 (36) at $p_T = 3$ GeV (20 GeV) in normalization, while its relative shifts due to IC are greatly reduced for the BHPS and meson-cloud models, as expected.

V. CONCLUSIONS

In this paper, we updated and improved our previous analysis [5] of charmed-meson inclusive hadroproduction at NLO in the GM-VFNS by using as input the non-perturbative FFs extracted from a global analysis of e^+e^- annihilation data from CESR [11], KEKB [12], and LEP1 [9, 10, 24] in the very same scheme [13]. In fact, this led to a significantly better description of the p_T distributions of the D^0, D^+, and D^{*+} mesons measured at the Tevatron [1], as becomes evident by comparing Figs. 1 and 2 with Figs. 1 and 2 in Ref. [5].

Encouraged by this finding, we then investigated how much room there is for the incorporation of IC inside the colliding hadrons. Specifically, we adopted six IC parameterizations [20], which are based on the BHPS [17], meson-cloud [18], and sea-like [20] models, implemented with two different values of $\langle x \rangle_{c+\overline{c}}$ each. For definiteness, we focused on the D^0

meson. In the case of the Tevatron, we found that the BHPS and meson-cloud models yield insignificant deviations from the zero-IC predictions, while the shift produced by the sea-like model is comparable to the experimental error and tends to worsen the agreement between theory and experiment. However, the experimental errors in Ref. [1] are still too sizeable to rule out this model as implemented in Ref. [20]. This is likely to change once the full data sample of run II is exploited.

Since IC typically receives a large fraction x of momentum from the parent hadron and the kinematical upper bound on x scales with $x_T = 2p_T/\sqrt{s}$, the sensitivity to IC may be enhanced by lowering the cm. energy $\sqrt{s}$. This is a strong motivation for studying the inclusive production of charmed mesons with large values of p_T in pp collisions at RHIC, currently operated at $\sqrt{s} = 200$ GeV. In fact, we found that all three IC models predict sizeable enhancements of the p_T distributions of D^0 mesons at RHIC, by up to 75% at $p_T = 10$ GeV. We, therefore, encourage our colleagues at RHIC to perform a dedicated study of charmed-meson inclusive production in the high-p_T regime. In a future high-energy pp-collision mode of RHIC, with $\sqrt{s} = 500$ GeV, which is to accrue more luminosity, the cross sections would be increased, while the relative shifts due to IC would be considerably smaller for the BHPS and meson-cloud models.

Acknowledgment

This work was supported in part by the German Federal Ministry for Education and Research BMBF through Grant No. 05 HT6GUA, by the German Research Foundation DFG through Grant No. KN 365/7–1, and by the Helmholtz Association HGF through Grant No. Ha 101.

---

[1] CDF Collaboration, D. E. Acosta *et al.*, Phys. Rev. Lett. **91**, 241804 (2003) [arXiv:hep-ex/0307080].

[2] PHENIX Collaboration, A. Adare *et al.*, Phys. Rev. Lett. **97**, 252002 (2006) [arXiv:hep-ex/0609010].

[3] STAR Collaboration, B. I. Abelev *et al.*, Phys. Rev. Lett. **98**, 192301 (2007) [arXiv:nucl-ex/0607012].

[4] STAR Collaboration, J. Adams *et al.*, Phys. Rev. Lett. **94**, 062301 (2005) [arXiv:nucl-ex/0407006].

[5] B. A. Kniehl, G. Kramer, I. Schienbein, and H. Spiesberger, AIP Conf. Proc. **792**, 867 (2005) [arXiv:hep-ph/0507068]; Phys. Rev. Lett. **96**, 012001 (2006) [arXiv:hep-ph/0508129]; B. A. Kniehl, in *Proceedings of the 14th International Workshop on Deep Inelastic Scattering (DIS 2006)*, Tsukuba, Japan, 2006, edited by M. Kuze, K. Nagano, and K. Tokushuku (World Scientific, Singapore, 2007) p. 573 [arXiv:hep-ph/0608122].

[6] B. A. Kniehl, G. Kramer, I. Schienbein, and H. Spiesberger, Phys. Rev. D **71**, 014018 (2005) [arXiv:hep-ph/0410289]; Eur. Phys. J. C **41**, 199 (2005) [arXiv:hep-ph/0502194].

[7] CTEQ Collaboration, J. Pumplin, D. R. Stump, J. Huston, H. L. Lai, P. Nadolsky, and W. K. Tung, J. High Energy Phys. 07 (2002) 012 [arXiv:hep-ph/0201195]; CTEQ Collaboration, D. Stump, J. Huston, J. Pumplin, W. K. Tung, H. L. Lai, S. Kuhlmann, and J. F. Owens, J. High Energy Phys. 10 (2003) 046 [arXiv:hep-ph/0303013].

[8] B. A. Kniehl and G. Kramer, Phys. Rev. D **74**, 037502 (2006) [arXiv:hep-ph/0607306].

[9] OPAL Collaboration, G. Alexander *et al.*, Z. Phys. C **72**, 1 (1996).

[10] OPAL Collaboration, K. Ackerstaff *et al.*, Eur. Phys. J. C **1**, 439 (1998) [arXiv:hep-ex/9708021].

[11] CLEO Collaboration, M. Artuso *et al.*, Phys. Rev. D **70**, 112001 (2004) [arXiv:hep-ex/0402040].

[12] Belle Collaboration, R. Seuster *et al.*, Phys. Rev. D **73**, 032002 (2006) [arXiv:hep-ex/0506068].

[13] T. Kneesch, B. A. Kniehl, G. Kramer, and I. Schienbein, Nucl. Phys. **B799**, 34 (2008) [arXiv:0712.0481 [hep-ph]]; B. A. Kniehl, in *Proceedings of the XVI International Workshop on Deep-Inelastic Scattering and Related Subjects (DIS 2008)*, London, England, 2008, edited by R. Devenish and J. Ferrando (Science Wise Publishing, Amsterdam, 2008), `http://dx.doi.org/10.3360/dis.2008.195` [arXiv:0807.2215 [hep-ph]].

[14] CTEQ Collaboration, W. K. Tung, H. L. Lai, A. Belyaev, J. Pumplin, D. Stump, and C. P. Yuan, J. High Energy Phys. 02 (2007) 053 [arXiv:hep-ph/0611254].

[15] R. S. Thorne, A. D. Martin, and W. J. Stirling, in *Proceedings of the 14th International Workshop on Deep Inelastic Scattering (DIS 2006)*, Tsukuba, Japan, 2006, edited by M. Kuze, K. Nagano, and K. Tokushuku (World Scientific, Singapore, 2007) p. 81 [arXiv:hep-ph/0606244].

[16] LHAPDF, the Les Houches Accord PDF Interface, URL:

http://projects.hepforge.org/lhapdf/pdfsets.

[17] S. J. Brodsky, P. Hoyer, C. Peterson, and N. Sakai, Phys. Lett. B **93**, 451 (1980); S. J. Brodsky, C. Peterson, and N. Sakai, Phys. Rev. D **23**, 2745 (1981).

[18] F. S. Navarra, M. Nielsen, C. A. A. Nunes, and M. Teixeira, Phys. Rev. D **54**, 842 (1996) [arXiv:hep-ph/9504388]; S. Paiva, M. Nielsen, F. S. Navarra, F. O. Duraes, and L. L. Barz, Mod. Phys. Lett. A **13**, 2715 (1998) [arXiv:hep-ph/9610310]; W. Melnitchouk and A. W. Thomas, Phys. Lett. B **414**, 134 (1997) [arXiv:hep-ph/9707387]; F. M. Steffens, W. Melnitchouk, and A. W. Thomas, Eur. Phys. J. C **11**, 673 (1999) [arXiv:hep-ph/9903441].

[19] E. Hoffmann and R. Moore, Z. Phys. C **20**, 71 (1983); B. W. Harris, J. Smith, and R. Vogt, Nucl. Phys. **B461**, 181 (1996) [arXiv:hep-ph/9508403].

[20] J. Pumplin, H. L. Lai, and W. K. Tung, Phys. Rev. D **75**, 054029 (2007) [arXiv:hep-ph/0701220].

[21] V. P. Goncalves, F. S. Navarra, and T. Ullrich, arXiv:0805.0810 [hep-ph].

[22] P. D. Thompson, J. Phys. G **34**, N177 (2007) [arXiv:hep-ph/0703103].

[23] J. Binnewies, B. A. Kniehl, and G. Kramer, Phys. Rev. D **58**, 014014 (1998) [arXiv:hep-ph/9712482].

[24] ALEPH Collaboration, R. Barate *et al.*, Eur. Phys. J. C **16**, 597 (2000) [arXiv:hep-ex/9909032].

[25] B. A. Kniehl and G. Kramer, Phys. Rev. D **71**, 094013 (2005) [arXiv:hep-ph/0504058].

[26] M. G. Bowler, Z. Phys. C **11**, 169 (1981).

[27] S. J. Brodsky, Few Body Syst. **36**, 35 (2005) [arXiv:hep-ph/0411056].

[28] J. Pumplin, Phys. Rev. D **73**, 114015 (2006) [arXiv:hep-ph/0508184].

[29] J. F. Donoghue and E. Golowich, Phys. Rev. D **15**, 3421 (1977).

[30] F. Aversa, P. Chiappetta, M. Greco, and J. P. Guillet, Phys. Lett. B **210**, 225 (1988); **211**, 465 (1988); Nucl. Phys. B **327**, 105 (1989).